Electron backscatter diffraction (EBSD) study of elongatoolithid eggs from China with microstructural and parataxonomic implications

Xufeng Zhu[1,2,3] (iD), Qiang Wang[1] and Xiaolin Wang[1,3,4]

[1]Key Laboratory of Vertebrate Evolution and Human Origins of Chinese Academy of Sciences, Institute of Vertebrate Paleontology and Paleoanthropology, Chinese Academy of Sciences, 100044 Beijing, China.
[2]National Natural History Museum of China, 100050 Beijing, China.
[3]College of Earth and Planetary Sciences, University of Chinese Academy of Sciences, 100049 Beijing, China.
[4]Centre for Research and Education on Biological Evolution and Environment, Nanjing University, 210023 Nanjing, China.

Non-technical Summary

In this study, we performed further microstructural studies of the eggshells of elongatoolithid eggs from China. We found that more diverse calcite crystal morphologies exist in these eggshells than were previously known. While excluding pathological structures, we also found evidence that some eggshells previously identified as elongatoolithid actually do not belong to this group. This study provides important data for the comparison of related fossil and extant eggshells.

Abstract

Electron backscatter diffraction (EBSD) has been widely used in recent studies of eggshells for its convenience in collecting in situ crystallographic information. China has a wide variety of dinosaur eggshells, although nearly none have been studied with this technique. Elongatoolithid eggs include many oogenera, although the microstructural differences of some were not highly appreciated, leading to several parataxonomic problems. In this paper, we surveyed seven elongatoolithid oogenera in China using EBSD in order to acquire more information about their microstructural variation. It is shown in this paper that in some elongatoolithid eggshells, scaly calcite grains that form the squamatic ultrastructure are not the only form of calcite in the continuous layer. Large columnar grains separated by high-angled grain boundaries and slender subgrains separated by radially arranged low-angled grain boundaries could exist in certain areas of the eggshells such as *Macroolithus* and *Macroelongatoolithus*. This paper discusses the criteria for identifying squamatic ultrastructure and proposes type I (rich in rugged high-angled grain boundaries) and type II (rich in both rugged high- and low-angled grain boundaries) squamatic ultrastructures. A pathological layer is found in *Undulatoolithus pengi*. An external zone is identified in the eggshell of *Heishanoolithus changii*, which does not support its position within the oofamily Elongatoolithidae. We argue that *Paraelongatoolithus* no longer belongs to Elongatoolithidae based on a combination of reticulated ornamentation, columnar continuous layer, and acicular mammillae. The high structural variation in elongatoolithid eggshells also implies that it may be inappropriate to relate all previous elongatoolithid eggshells to oviraptorosaurs and assume they are non-monophyletic.

Introduction

Electron backscatter diffraction (EBSD) is a powerful tool for in situ quantitative analysis of crystalline materials. An EBSD detector is attached to a scanning electron microscope (SEM) to obtain a Kikuchi pattern, allowing automatic analysis of grain orientations, local textures, point-to-point orientation correlations, and phase identification and distribution (Schwarzer et al. 2009). Geologists also apply this technique in different fields in the Earth sciences (Prior et al. 2009), including paleontology. This method has been applied by paleontologists in studies of biocrystalline materials like coral reefs (Cusack et al. 2008b; Cusack 2016) and mollusk shells (Cusack et al. 2008a; Pérez-Huerta et al. 2011). Sauropsid eggshells are typical biocrystalline materials (Mikhailov 2019) and therefore are well-suited for EBSD study. Dalbeck and Cusack (2006) first studied modern avian eggshells with EBSD to explore the relationship between the distribution of trace elements and the crystallographic structures of the eggshell, and this technique was soon applied to eggshells of non-avian dinosaurs (Grellet-Tinner et al. 2011; Trimby and Grellet-Tinner 2011; Moreno-Azanza et al. 2013,

2016, 2017; Eagle et al. 2015; Choi et al. 2019, 2022a; Choi and Lee 2019; Kim et al. 2019; Oser et al. 2021; Han et al. 2023), other birds (Grellet-Tinner et al. 2012, 2016, 2017; Jain et al. 2016; Pérez-Huerta and Dauphin 2016; Dauphin et al. 2018; Choi et al. 2023), and other sauropsids (Choi et al. 2018, 2022b,c; Choi 2020; Moreno-Azanza et al. 2021; Xu et al. 2022; Wu et al. 2023). For fossil eggshells, EBSD can be used to examine the extent of diagenesis to exclude nonbiological structures (Eagle et al. 2015; Moreno-Azanza et al. 2016). Shape and size of calcite grains can be directly displayed in Euler and grain boundary (GB) maps, allowing identification of structures that could be neglected with a traditional method like polarized light microscopy. The usefulness of EBSD examination has been shown in some ootaxa, and it also has potential in the parataxonomic study of eggshells.

Elongatoolithid eggs, represented by *Elongatoolithus* (Zhao 1975; Zhao et al. 2015), include many ootaxa from Asia and North America. These eggs are characterized by their elongated shape and ornamented eggshell with two structural layers (mammillary layer and continuous layer) and radially arranged paired eggs in layered rings (Zhao 1975; Yang et al. 2019). Mikhailov (1997b) refined the diagnosis of the eggshell of Elongatoolithidae, which has a ratite morphotype, angusticanaliculate pore system, linearituberculate ornamentation on the equatorial part of the egg, and dispersituberculate ornamentation on the poles. The continuous layer of elongatoolithid eggshell lacks an external ultrastructural zone; therefore, the range of the continuous layer also represents the range of its squamatic zone (Mikhailov 1997b).

Several problems exist in the study of parataxonomy of elongatoolithid eggs. An important question is whether this group is monophyletic. Taxonomically, three elongatoolithid oogenera (*Elongatoolithus*, *Macroolithus*, and *Macroelongatoolithus*) have been related with oviraptorosaurs based on strong evidence (Sato et al. 2005; Weishampel et al. 2008; Pu et al. 2017), while the oogenus *Paraelongatoolithus* is considered to be similar to the eggs of dromaeosaurs (Grellet-Tinner and Makovicky 2006; Wang et al. 2010a; Choi and Lee 2019), which clearly makes the oofamily Elongatoolithidae polyphyletic. Some oogenera like *Undulatoolithus* (Wang et al. 2013) and *Heishanoolithus* (Zhao and Zhao 1999) were rarely studied or described, making comparison of other ootaxon with these oogenera impractical.

This study aims to acquire microstructural and crystallographic characteristics that were overlooked in former studies by applying polarizing light microscopy (PLM), SEM, and EBSD to seven representative elongatoolithid oogenera from China. The newly observed features provide more objective prerequisites to discuss the aforementioned parataxonomic problems.

Materials and Methods

Seven elongatoolithid oospecies were selected for study, including *Elongatoolithus elongatus* (IVPP V 734), *Macroolithus yaotunensis* (IVPP V 2781) (Zhao 1975), *Heishanoolithus changii* (IVPP V 11578) (Zhao and Zhao 1999), *Undulatoolithus pengi* (PXM V 0016) (Wang et al. 2013), *Paraelongatoolithus reticulatus* (IVPP V 16514) (Wang et al. 2010a), *Nanhsiungoolithus chuetienensis* (IVPP V 2783) (Zhao 1975), and *Macroelongatoolithus xixiaensis* (TTM 15) (Wang et al. 2010b). All eggshell samples are housed in IVPP.

The only *U. pengi* clutch, PXM V 0016, contains five complete eggs and three broken eggs (Supplementary Fig. 13). Six eggs in the clutch were sampled and thin sectioned to study the microstructural variation among eggs in the clutch. The clutch is housed in PXM.

Some of the specimens were thin sectioned in the original studies, and the remaining resin blocks were sufficient for sample preparation for EBSD analysis. As for those without remaining resin blocks, new samples were taken from the specimens for both thin section preparation and EBSD analysis. The eggshells were thin sectioned down to 30 μm following standard procedures (Zhu et al. 2021) (Fig. 1), and the remaining resin blocks were then used for EBSD analysis. Thin sections were observed and photographed with a Zeiss Axio imager A2m polarized light microscope, and both normal and cross-polarized light were used (Fig. 1).

Elongatoolithid eggs usually have linear extended ornamentation (ridge or nodes, especially in the equatorial region; Mikhailov 1997b); therefore, analyses were made on sections that are perpendicular to the extension direction of the ornamentation for comparison.

Resin blocks with radial sections exposed after thin sectioning were polished for EBSD analysis. The preparation process was similar to that followed by previous researchers (Moreno-Azanza et al. 2013; Choi et al. 2019). The surface to be observed for each sample was ground with silicon carbide abrasive paper using an EXAKT 400CP variable speed grinder-polisher in order to obtain a flat observation surface; then it was polished with 1 μm (5 min) and 0.25 μm (5 min) diamond suspension to remove scratches before finally being polished with 0.04 μm (10 min) and 0.02 μm (10 min) colloidal silica on a polishing cloth to remove superficial damage. The polished sample was then coated with 4–5 nm carbon to make the sample conductive, which is also thin enough to ensure the quality of the Kikuchi diffraction pattern (Pérez-Huerta and Cusack 2009). The block was stuck to the sample stage by carbon tape, with its sample surface tilted by 70°. The EBSD analyses were performed with an Oxford Nordlys Nano EBSD detector attached to a field emission SEM (Nova NanoSEM 450, housed in IGGCAS), and the Kikuchi patterns were analyzed with AZtec software. The scanning settings include 20 kV accelerating voltage, 80 nA beam current, and 18 mm working distance. The scanning step size ranged from 2 to 6 μm.

GB maps were obtained under thresholds of 5°, 10°, and 20°, representing the lower limit of low-, medium-, and high-angled GB, respectively. The noise reduction procedure for GB maps included wild spike elimination and one step of zero solution correction (i.e., a pixel is surrounded by eight pixels, and if six of them have the same value, then the center pixel, which might have no data as "zero solution," is set to that value). Euler and IPF-Y (red pixels represent calcite grains that have the c-axis pointed to the outer surface) maps were obtained with raw data.

The secondary calcite data were removed before the generation of misorientation histograms and pole figures. Misorientation histograms were acquired with the lower limit of 5° and a step width of 2.5°. Misorientation angle distributions of correlated and uncorrelated pairs were obtained and graphed under the same noise reduction procedure used in GB maps. Pole figures were present in both scattered dots and contours (10° half width and 3° cluster size).

SEM observations were first made on fresh fracture surfaces and then on acid-treated (5% acetic acid, 1 min) fracture surfaces. The observations were performed with a Zeiss EVO MA 25 SEM housed in IVPP. The scanning settings include 10 kV accelerating voltage, 5 pA beam current, and 7 to 10 mm working distance.

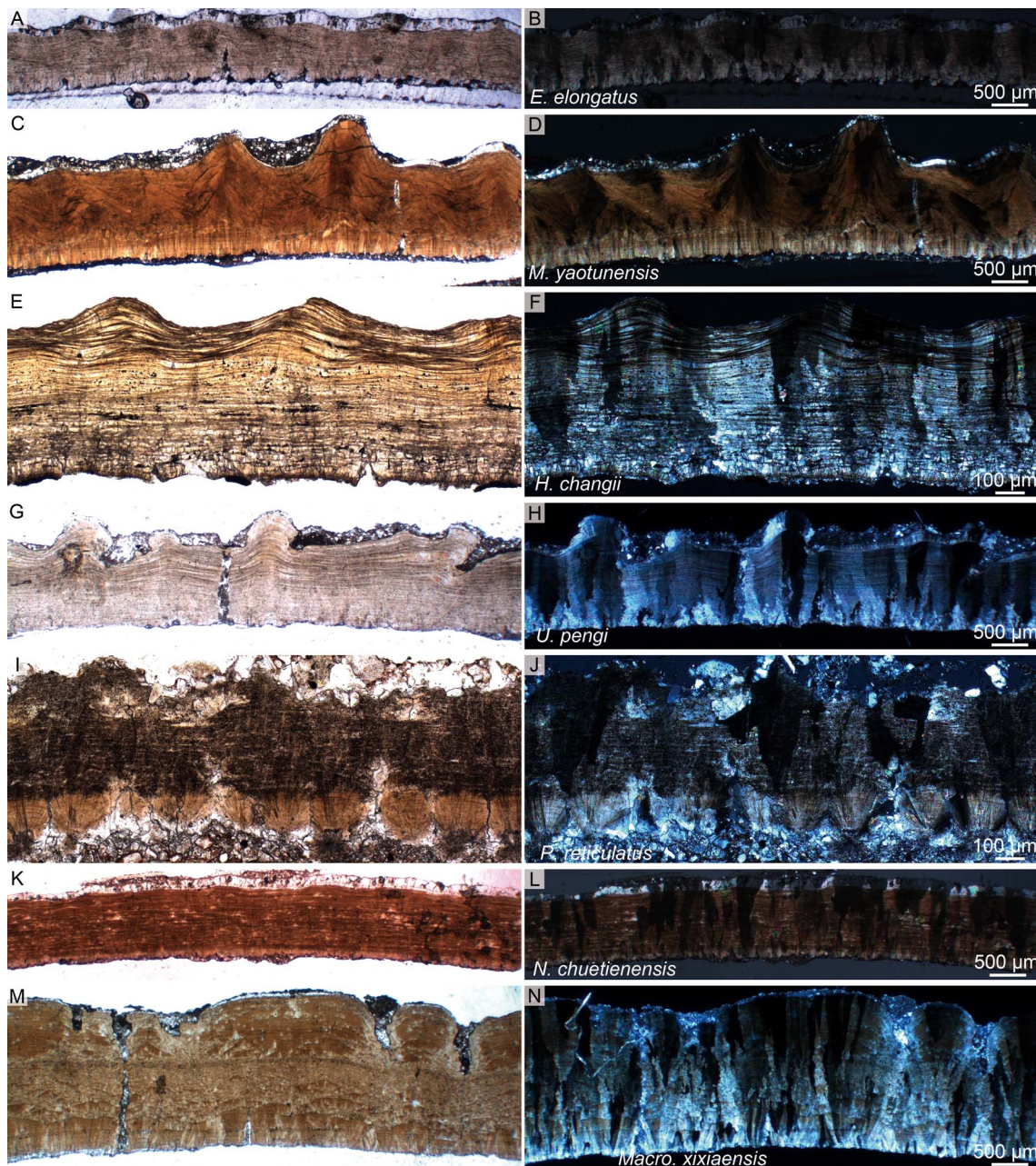Anatomical terminology in this paper follows Mikhailov (1997b).

Figure 1. Thin sections of the eggshells under normal (left) and cross-polarized light (right). A, B, *Elongatoolithus elongatus* (IVPP V 734); C, D, *Macroolithus yaotunensis* (IVPP V 2781); E, F, *Heishanoolithus changii* (IVPP V 11578); G, H, *Undulatoolithus pengi* (PXM V 0016); I, J, *Paraelongatoolithus reticulatus* (IVPP V 16514); K, L, *Nanhsiungoolithus chuetienensis* (IVPP V 2783); M, N, *Macroelongatoolithus xixiaensis* (TTM 15).

Institutional Abbreviations

IVPP, Institute of Vertebrate Paleontology and Paleoanthropology, Chinese Academy of Sciences, Beijing, China; **IGGCAS**, Institute of Geology and Geophysics, Chinese Academy of Sciences; **PXM**, Pingxiang Museum, Pingxiang, Jiangxi Province, China; **TTM**, Tiantai Museum, Tiantai, Zhejiang Province, China.

Results

Preservation State

IPF-Y maps were used to characterize the c-axis orientation of calcite grains. The IPF-Y map is useful in identifying diagenetic structures (Cusack et al. 2008b; Moreno-Azanza et al. 2013,

2016; Eagle et al. 2015; Choi and Lee 2019; Choi et al. 2019). All examined specimens show a regularly arranged c-axis of calcite grains, which have more oblique or horizontal grains in the mammillary layer (shows more blue and green in IPF-Y maps) and more grains aligned toward the outer surface in the continuous layer (red in IPF-Y maps) (Fig. 2). The results indicate that the grain orientation of all seven specimens are basically original rather than having undergone severe diagenetic processes. The calcite crystals of all specimens are more dispersed in the lower part and are more aligned in the upper part (Supplementary Figs. 3, 7, 11, 17, 22, 26, 30), which are normal for the growth of most amniotic eggshells (Moreno-Azanza et al. 2013, 2017) except for gecko eggshells (Choi et al. 2018). The examination of crystallographic orientation adds to the usability of data, allowing reliable interpretation.
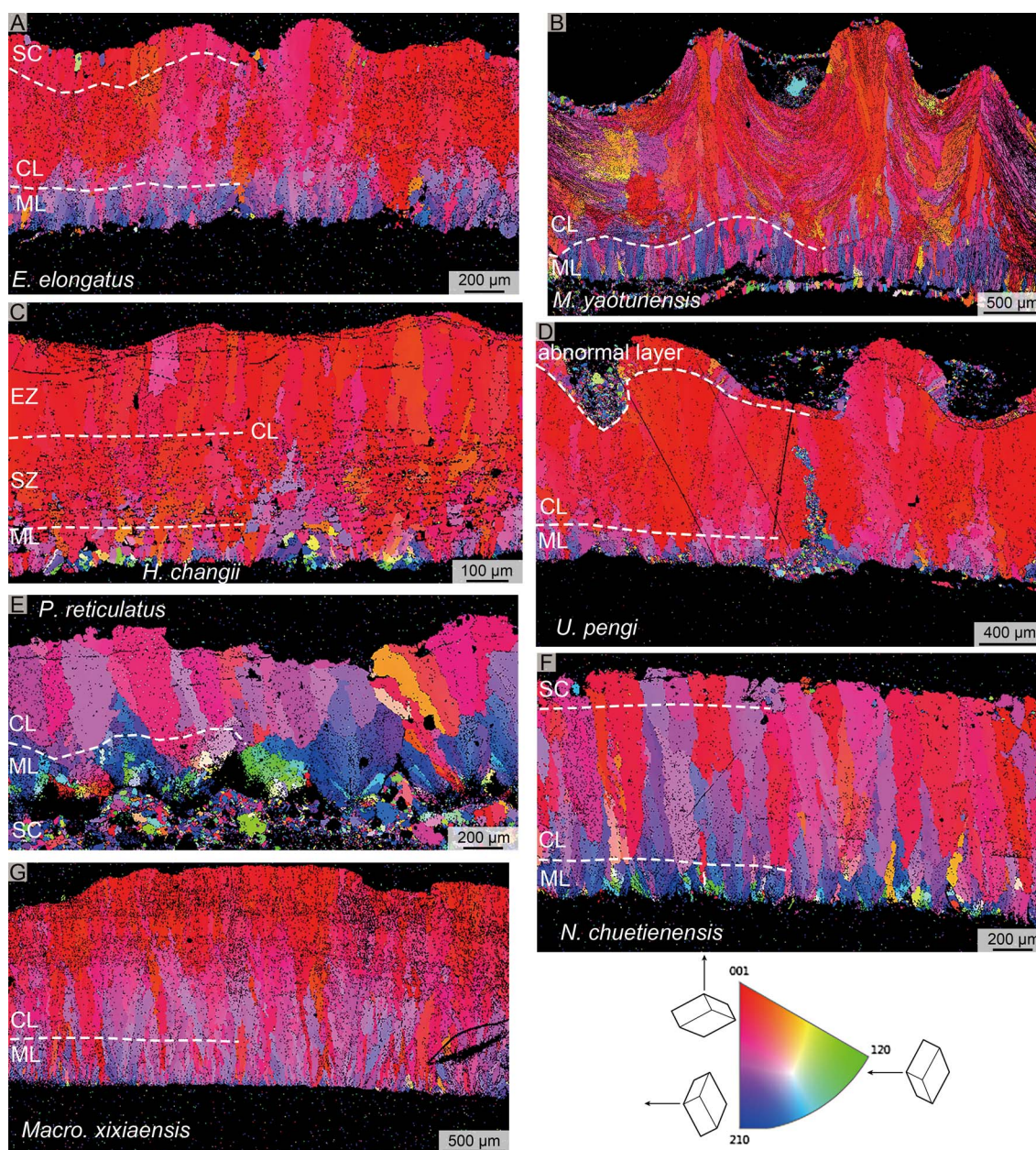
Figure 2. IPF-Y maps of the eggshells. A, *Elongatoolithus elongatus* (IVPP V 734); B, *Macroolithus yaotunensis* (IVPP V 2781); C, *Heishanoolithus changii* (IVPP V 11578); D, *Undulatoolithus pengi* (PXM V 0016); E, *Paraelongatoolithus reticulatus* (IVPP V 16514); F, *Nanhsiungoolithus chuetienensis* (IVPP V 2783); G, *Macroelongatoolithus xixiaensis* (TTM 15). Red pixels indicate c-axis vertical to the outer surface, while green and blue pixels indicate c-axis parallel to the outer surface. CL, continuous layer; ML, mammillary layer; SZ, squamatic zone; EZ, external zone; SC, secondary calcite.

Secondary calcite grains present in the eggshells of *Elongatoolithus elongatus* (Figs. 3A, 4A, Supplementary Fig. 1A) and *Nanhsiungoolithus chuetienensis* (Figs. 3F, 4F, Supplementary Fig. 24A) exhibit syntaxial overgrowth.

Morphology and Arrangement of Calcite Grains

The combined use of IPF-Y, Euler, and GB maps allowed detailed characterization of the orientation, morphology and arrangement of the calcite crystals in the eggshells.

Though the bottom of the mammillary layer was not completely preserved, *Elongatoolithus elongatus* shows gradual transition between the mammillary and continuous layer under normal light (Supplementary Fig. 1A). The mammillae in the mammillary layer are closely arranged, and each is composed of radiating wedges (Supplementary Fig. 1C). In the continuous layer, the calcite crystallites inlay with each other and are separated by rugged GBs (Figs. 3A, 4A). In the scanned area, most of the GBs in the continuous layer were high-angled, although there are also areas that are rich in low-angled GBs. The squamatic grains show irregular extinction under cross-polarized light (Supplementary Fig. 1B,F), which reflects typical squamatic ultrastructure. The surface is moderately undulating (Fig. 1A) due to the presence of linear ridges (Young 1954: plate I, fig. 1; Zhao 1975; Zhao et al. 2015: fig. 14).

Macroolithus yaotunensis has a distinct boundary between the mammillary and continuous layer under normal light (Supplementary Fig. 5C), which is more abrupt than that of
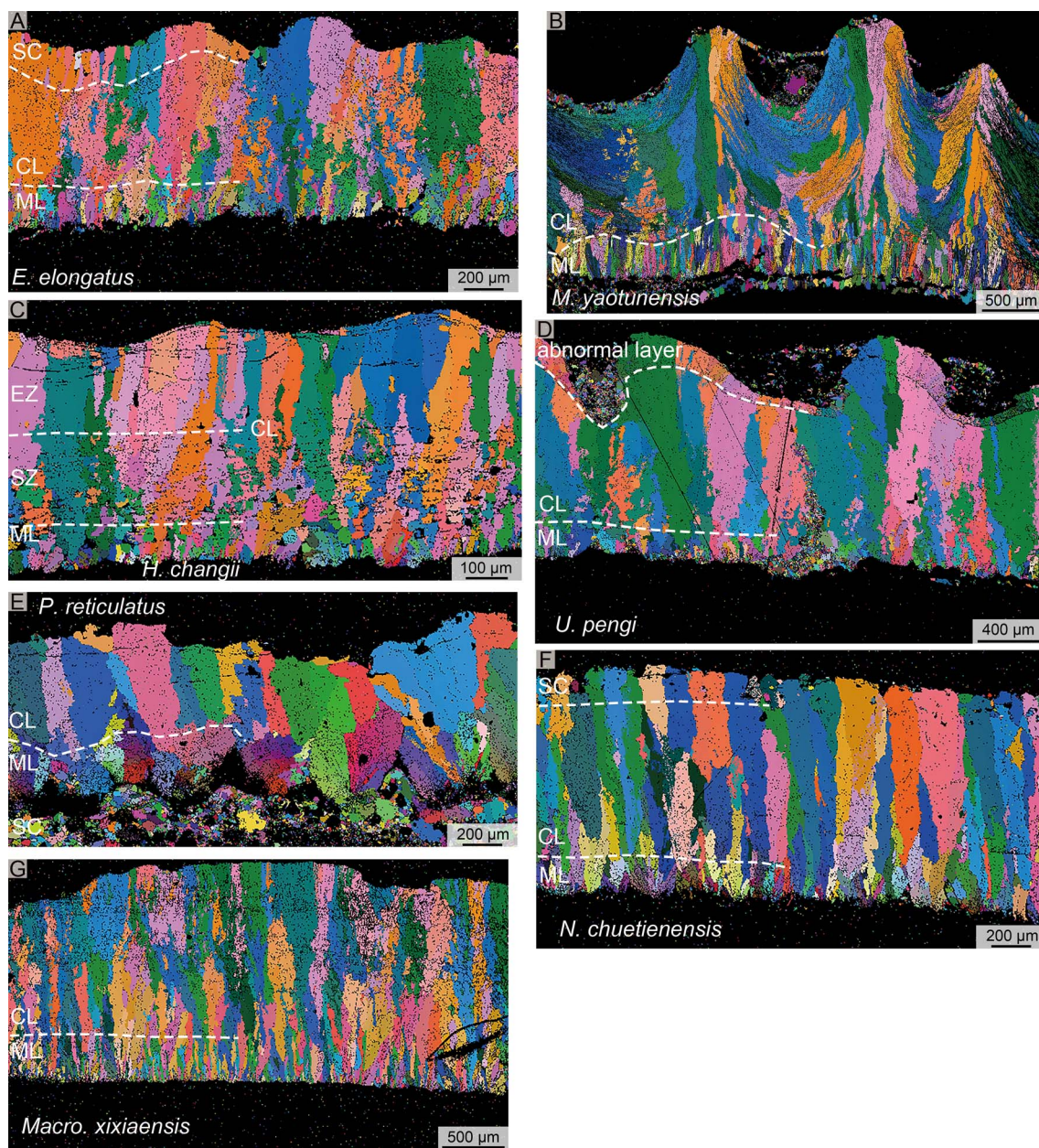
Figure 3. Euler maps of the eggshells. A, *Elongatoolithus elongatus* (IVPP V 734); B, *Macroolithus yaotunensis* (IVPP V 2781); C, *Heishanoolithus changii* (IVPP V 11578); D, *Undulatoolithus pengi* (PXM V 0016); E, *Paraelongatoolithus reticulatus* (IVPP V 16514); F, *Nanhsiungoolithus chuetienensis* (IVPP V 2783); G, *Macroelongatoolithus xixiaensis* (TTM 15). CL, continuous layer; ML, mammillary layer; SZ, squamatic zone; EZ, external zone; SC, secondary calcite.

Elongatoolithus and is the major diagnostic characteristic of *Macroolithus* (Zhao 1975). The boundary can be well defined by the abrupt change of grain orientation (Fig. 2B) or GBs (Fig. 4B). The mammillary layer of *M. yaotunensis* is composed of compactly arranged mammillae that consist of radially arranged slender calcite wedges. The continuous layer of *M. yaotunensis*, however, is not simply composed of calcite grains that have their c-axes aligned with their long axes. Three morphological types of calcite grains exist in the continuous layer of *M. yaotunensis* (Fig. 4B). Type A (Fig. 4B) consists of small scaly calcite crystallites that are most abundant in the continuous layer, the c-axes of which are nearly perpendicular to the outer surface (Fig. 2B), while the extending directions of the grains are aligned with the undulation of the accretion lines (Figs. 3B,

4B). The squamatic crystallites are separated by rugged high-angled GBs, while rugged low-angled GBs are also developed in each one, forming squamatic subgrains and indicating strong presence of squamatic ultrastructure. Type B (Fig. 4B) exists only below the center of ridges as several large prismatic crystallites that are gathered together. High-angled GBs that are not rugged separate these prisms, and low-angled GBs are nearly absent in the prisms. The prisms show columnar extinction (Supplementary Fig. 5F), and squamatic ultrastructure is also absent and replaced by parallel cleavages under an SEM (Supplementary Fig. 6C). It is also possible to identify this structure under plain light, as the accretion lines are more parallel (Supplementary Fig. 5E). The prismatic columns also cause the constriction of accretion lines beneath the ridges, where the
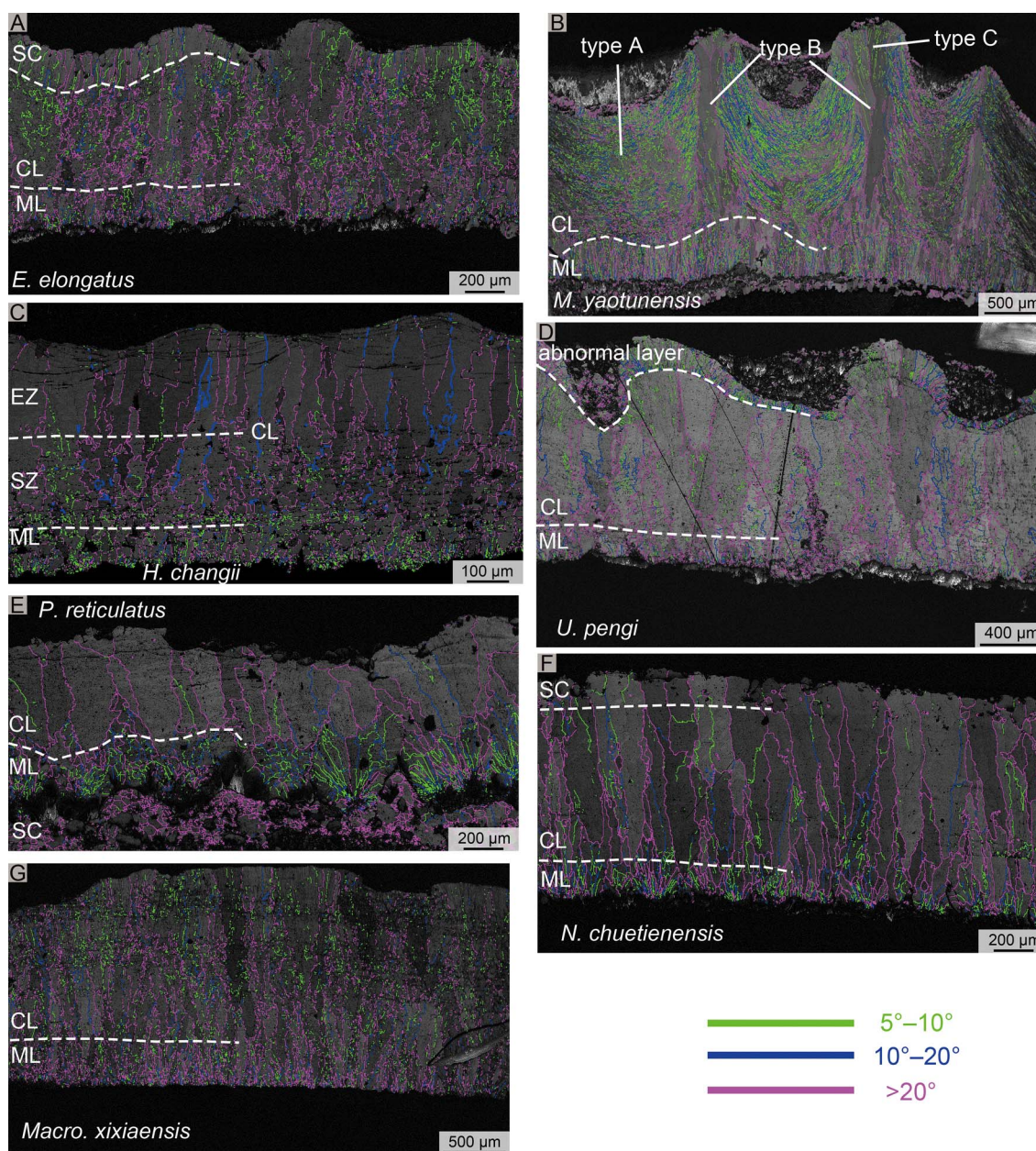
Figure 4. Grain boundary (GB) maps of the eggshells. A, *Elongatoolithus elongatus* (IVPP V 734); B, *Macroolithus yaotunensis* (IVPP V 2781); C, *Heishanoolithus changii* (IVPP V 11578); D, *Undulatoolithus pengi* (PXM V 0016); E, *Paraelongatoolithus reticulatus* (IVPP V 16514); F, *Nanhsiungoolithus chuetienensis* (IVPP V 2783); G, *Macroelongatoolithus xixiaensis* (TTM 15). Green (5–10°), blue (10–20°), and purple (above 20°) lines stand for low-, medium-, and high-angled GBs, respectively. CL, continuous layer; ML, mammillary layer; SZ, squamatic zone; EZ, external zone; SC, secondary calcite.

accretion lines seems to be jacked up toward the top of an ornamentation (Supplementary Fig. 5E). However, it is possible that this structure may not show up in some thin sections or under some ridges because the position of the section can occasionally deviate from the center of ridges; therefore, a thin section with proper orientation and field of view width would decrease the probability of misidentification. Type C (Fig. 4B) consists of bunches of radially arranged slender calcite subgrains that usually originated near the top of the prisms of the second type and extend to the tops of ridges. These slender calcite subgrains are separated by linear low-angled GBs, and show sweeping extinction under cross-polarized light (Supplementary Fig. 5F). The undulation near the surface is strong, but can be weak in some

places (Fig. 1C), because the sections do not always cut through the peak of a node (Young 1965: plates I–III; Zhao 1975; Zhao et al. 2015: fig. 18).

The first layer of *Heishanoolithus changii* is the mammillary layer, and its structure is very similar to that of *E. elongatus*, whose upper border is also gradual (Supplementary Fig. 1A,C). The second layer is the continuous layer; however, unlike any other specimens in this study, the continuous layer of *H. changii* consists of two zones (Fig. 2C). The inner zone shows irregular extinction (Supplementary Fig. 9D) that is similar to the continuous layers of *E. elongatus* and *M. yaotunensis*, which show squamatic ultrastructure (Supplementary Fig. 10B). Therefore, this zone can be clearly identified as the squamatic zone. The GBs

in the squamatic zone are mostly high-angled and very rugged (Fig. 4C). The outer zone consists of a layer of compactly arranged calcite prisms that are separated by relatively straight high-angled GBs (Fig. 4C). Low-angled GBs are nearly absent in the outer zone. The outer zone therefore shows columnar extinction (Supplementary Fig. 9F), which appears to be very similar to the typical external zone in many avian eggs (Mikhailov 1997a). The accretion lines are more prominent and isolated in this part (Supplementary Fig. 9E). The surface undulation is similar to *Elongatoolithus* (Fig. 1E), although its surface ornamentation is composed of dense (but still dispersed) nodes that are approximately oriented along the longitudinal axis (Zhao and Zhao 1999: plate I, fig. 2).

In the sample of *Undulatoolithus pengi* (egg no. 6 in the clutch; Supplementary Fig. 13), an unexpected additional layer is clearly identified near the outer surface in the Euler map (Fig. 3D) and GB map (Fig. 4D). The boundary between the additional layer and the structure below is distinct: radiating GBs (both low- and high-angled) reoccur and extend to the outer surface of the eggshell (Fig. 4D). Most GBs in this layer are not continuous with those below. This additional structure can also be identified under cross-polarized light (Supplementary Fig. 14B), but could easily be overlooked when viewed under normal light, because it could be confused with the dense accretion lines, just as it was in the original literature (Wang et al. 2013). However, other sampled eggs (egg nos. 1–4, 7) do not have this structure (Supplementary Fig. 19B,D,F,H,L). We interpret this additional layer as an abnormal structure, as it is similar to some pathological structures in other fossil eggshells (Jackson et al. 2004; Grellet-Tinner et al. 2010); therefore, the rest of the eggshell was used for comparison and is described here. The mammillary layer of *U. pengi* is similar to that of *E. elongatus*, which is composed of compactly arranged mammillae that are composed of radiating wedges, and has a gradual boundary with the continuous layer (Supplementary Fig. 14C). The rugged GB in its continuous layer is not as rich as that in *E. elongatus* (Fig. 4D), and sweeping extinction (Supplementary Fig. 14E) appears just below the ornamentation with radially arranged calcite grains (Supplementary Fig. 15D). The rugged high-angled GBs are more perpendicular to the eggshell surface when presented in the outer part of the eggshell. The surface undulation of *U. pengi* is very strong (Fig. 1G), even in those samples without an abnormal layer (Supplementary Fig. 19A,C,E,G,K), reflecting its strong linearly arranged ridges and nodes (Wang et al. 2013: fig. 3). *Paraelongatoolithus reticulatus* has eggshell units that are less fused than those in other oospecies in this study, although they are not simply spherulites like those of the dinosauroid-spherulitic basic type. Each eggshell unit is composed of a fan-shaped mammilla with radially arranged slender calcite grains (Supplementary Fig. 20C) that are slimmer than all oogenera in this study except *Nanhsiungoolithus*, and large calcite wedges originate from the upper edge of mammillae and reach the outer surface (Fig. 4E). The mammilla of *Paraelongatoolithus* can be classified as acicular. There is a clear border between the mammillary and continuous layer (Supplementary Fig. 20A). The large wedges form the continuous layer and show columnar to slightly fan-shaped extinction (Supplementary Fig. 20B). Low-angled GBs are rich in the mammillae, but are nearly absent in the continuous layer. The wedges in the continuous layer are separated by rugged high-angled GBs that are extended vertically. The surface curvature is not fully complete due to possible erosion (Fig. 1I), but undulation is visible as a result of the reticulated ornamentation (Wang et al. 2010a: fig. 2A).

The eggshell of *N. chuetienensis* has broad mammillae that are looser than those of *Macroolithus* (Supplementary Fig. 24C), and each mammilla is composed of radially arranged calcite grains (Supplementary Fig. 24C) that are similar to those of *Paraelongatoolithus*. The continuous layer shows columnar extinction under cross-polarized light (Supplementary Fig. 24B,F) and consists of large but slender prismatic calcite grains that are separated by high-angled GBs that are perpendicular to the surface. Low-angled GBs are rare in the continuous layer (Fig. 4F). The GBs are less rugged than those in *E. elongatus* and *M. yaotunensis*. The surface undulation of *Nanhsiungoolithus* is very weak (Fig. 1K), which is consistent with the description of its smooth or faint ridged surface (Young 1965: plates XII, XIIIA; Zhao 1975; Zhao et al. 2015: fig. 20).

In *Macroelongatoolithus xixiaensis*, the mammillary layer is similar to that of *M. yaotunensis*. However, in this specimen, the upper border with the continuous layer is not very distinct compared with other specimens (Zelenitsky et al. 2000) or even other eggshells from different positions of TTM 15 (Wang et al. 2010b: fig. 4A). This is due to the stacked wedges on top of normal mammillae and the disordered blocky structure located at the lower part of the continuous layer (Supplementary Fig. 28A,C), which were interpreted as pathological structures by former researchers (Wang et al. 2010b). In the disordered area, the accretion lines are less developed and the GB map shows blocky grains separated by rugged high-angled GBs with few low-angled GBs inside the block (Fig. 4G). The upper part of the continuous layer is normal and has more prismatic calcite grains near the ornamentation (Supplementary Fig. 28E,F). The prismatic grains are separated by high-angled GBs, which are often slightly rugged. Rugged low-angled GBs are rich within the continuous layer, indicating the presence of squamatic ultrastructure. The low-angled GBs became straightly extended and radially arranged near the outer surface or at the location of ridges, forming radially arranged slender subgrains (Supplementary Fig. 28F) similar to those in *M. yaotunensis*. This specimen was located near the pointed end of the egg, and the surface undulation of this eggshell is very strong but slightly irregular (Fig. 1M), which is caused by the dense nodes on the surface (Wang et al. 2010b: fig. 3B).

Misorientation Angle Distribution

In general, all specimens studied show low-angled dominant correlated misorientation (Fig. 5), which is similar to the results of former research on elongatoolithid eggs (Choi et al. 2019). However, the distribution of high-angled correlated misorientation varies among these oospecies. High-angled correlated misorientation is lowest in *Macroolithus yaotunensis* (Fig. 5B), with only 39.88% above 20°, while it is higher in *Elongatoolithus elongatus* (64.27%; Fig. 5A), *Heishanoolithus changii* (65.02%; Fig. 5C), *Undulatoolithus pengi* (68.32%; Fig. 5D), *Paraelongatoolithus reticulatus* (59.81%; Fig. 5E), *Nanhsiungoolithus chuetienensis* (65.02%; Fig. 5F), and *Macroelongatoolithus xixiaensis* (62.16%; Fig. 5G). The significantly low proportion of high-angled correlated misorientation of *M. yaotunensis* is most likely to be the result of rich low-angled GBs in its eggshell (Fig. 4B).

In the meantime, it is inappropriate to compare misorientation between different eggshells, because the misorientation distribution of different structural layers can vary significantly in an eggshell; therefore misorientation distribution must be considered before being used for character coding. Taking misorientation histograms of different structural layers in an eggshell into
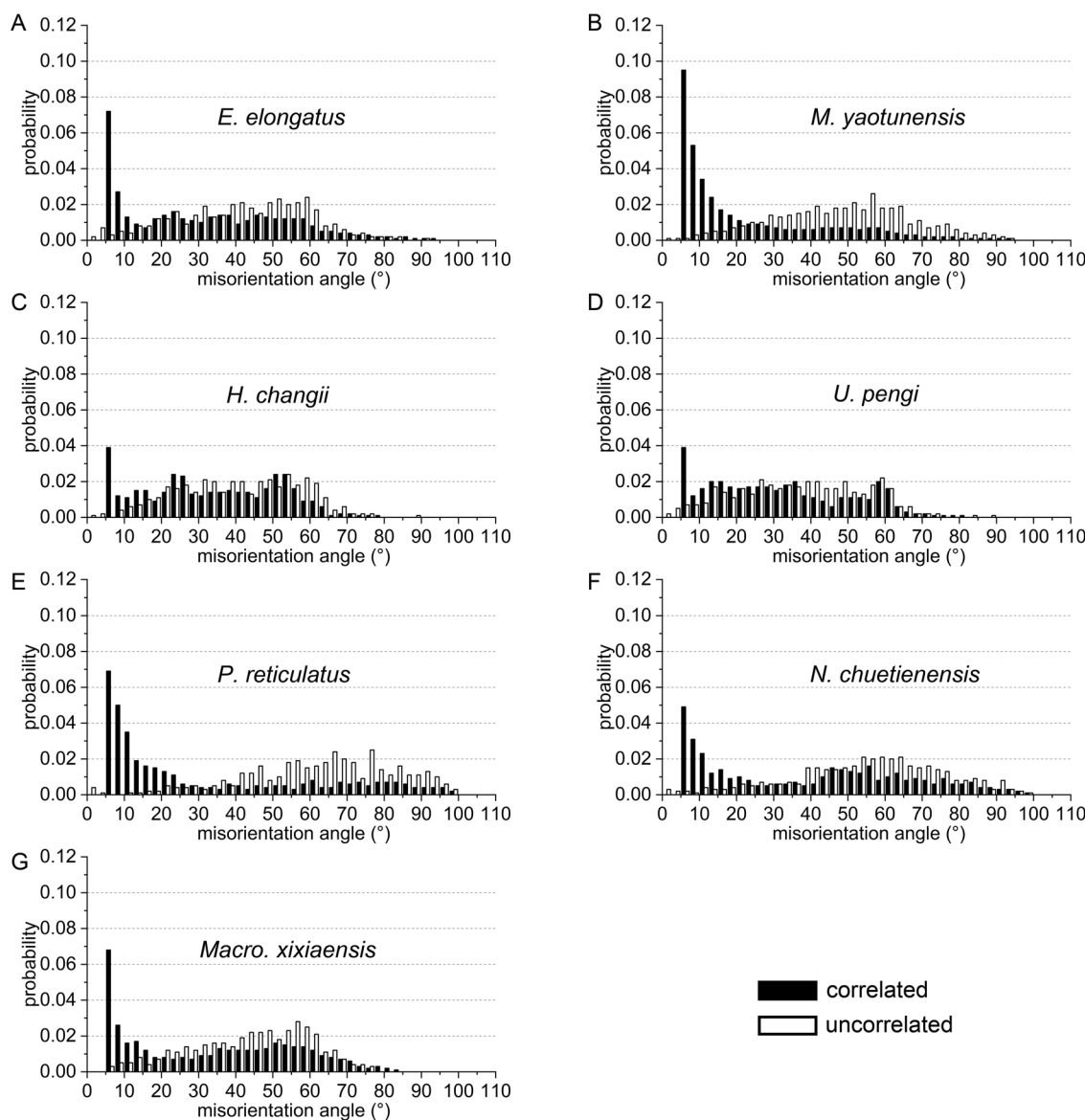
Figure 5. Misorientation histograms of the eggshells. A, *Elongatoolithus elongatus* (IVPP V 734); B, *Macroolithus yaotunensis* (IVPP V 2781); C, *Heishanoolithus changii* (IVPP V 11578); D, *Undulatoolithus pengi* (PXM V 0016); E, *Paraelongatoolithus reticulatus* (IVPP V 16514); F, *Nanhsiungoolithus chuetienensis* (IVPP V 2783); G, *Macroelongatoolithus xixiaensis* (TTM 15). Data from areas of matrix or secondary calcite were removed before analysis.

account, it is clearly shown that the low-angled misorientation distribution in *E. elongatus* (Supplementary Fig. 4), *M. yaotunensis* (Supplementary Fig. 8), and *M. xixiaensis* (Supplementary Fig. 31) is contributed to by the continuous layer, which is rich in low-angled GBs. In contrast, the mammillary layer contributed most of the low-angled misorientation in *H. changii* (Supplementary Fig. 12), *P. reticulatus* (Supplementary Fig. 23), and *N. chuetienensis* (Supplementary Fig. 27).

Discussion

Criteria for Two Squamatic Ultrastructure Types

Squamatic ultrastructure, characterized by a particular squamatic (scaly) pattern (Mikhailov 1997b), is regarded as an important structure that makes ornithoid-type eggshell distinct from any other type of eggshell (Mikhailov 2014), although it does not

appear to be clearly present in all fossil ornithoid-type eggshells. This structure is often observed in the continuous layer of some avian and non-avian dinosaur eggshells; therefore, the continuous layer is also commonly referred to as the squamatic zone in terms of ultrastructural zone, if the squamatic ultrastructure is shown. Usually, the identification of squamatic ultrastructure requires a section under an SEM, but it can also be identified by the extinction pattern through cross-polarized light through observation of a thin section under a polarized microscope (Mikhailov 1991), as an area with strong squamatic ultrastructure would show irregular extinction rather than sweeping or columnar extinction. Choi et al. (2019) offered an alternative way to visualize the distribution of squamatic ultrastructure by GB mapping through EBSD analysis, in which they suggested that the squamatic ultrastructure could be represented by the presence of rugged GBs. This definition is a good start to visually identify squamatic ultrastructure. Furthermore, on that basis, we would like to differentiate two

types of squamatic ultrastructure with EBSD by the general morphology and proportion of low-angled GBs in those rugged GBs.

Type I squamatic ultrastructure here is defined as areas of rugged high-angled GBs (Fig. 6A). This is basically the same as the definition of Choi et al. (2019), except for the absence of low-angled GBs. In extant Neognathae, the whole squamatic zone in the eggshell of domestic duck (*Anas platyrhynchos domesticus*), domestic chicken (*Gallus gallus domesticus*), Japanese tit (*Parus minor*), and Korean magpie (*Pica sericea*) (Choi et al. 2019) clearly shows this type. The squamatic zone in the eggshell of Australian brush turkey (*Alectura lathami*), malleefowl (*Leipoa ocellata*) (Grellet-Tinner et al. 2017), and American flamingo (*Phoenicopterus ruber*) (Grellet-Tinner et al. 2012) probably exhibits type I squamatic ultrastructure. A fossil neognath like a suggested Phoenicopteridae (Grellet-Tinner et al. 2012) also has a squamatic ultrastructure similar to that of *P. ruber* eggshell. In extant Palaeognathae, the whole squamatic zone of the eggshells of ostrich (*Struthio camelus*), emu (*Dromaius novaehollandiae*), cassowary (*Casuarius casuarius*), kiwi (*Apteryx mantelli*), tinamou (*Eudromia elegans* and *Nothoprocta perdicaria*), and the "thick moa eggshells" (*Dinornis*), as well as the inner part of the squamatic zone of the eggshells of rhea (*Rhea* sp.), elephant bird (Aepyornithidae), and the "thin and middle thickness moa eggshells" (Choi et al. 2023) show type I squamatic ultrastructure. A fossil palaeognath species *Lithornis vulturinus* (Grellet-Tinner and Dyke 2005; Choi et al. 2023) also shows type I squamatic ultrastructure in its eggshell, but note that there are possible diagenetically induced cleavages in its calcite grains (Choi et al. 2023: fig. 10C), which might have destroyed low-angled GBs. Fossil

non-avian dinosaur eggshells sometimes show this type of squamatic ultrastructure, such as *Prismatoolithus levis* (egg of *Troodon*) (Choi et al. 2019), *Trigonoolithus amoae* (Moreno-Azanza et al. 2013, 2014), *Protoceratopsidovum sincerum*, *Protoceratopsidovum fluxuosum* (Choi et al. 2022a) and the inner sublayer of *Reticuloolithus acicularis* (Choi and Lee 2019). *Gobioolithus minor* shows type I squamatic ultrastructure in its squamatic zone (Choi et al. 2019). However, this type of squamatic ultrastructure is qualitative, and could easily be interpreted differently, because the ruggedness of high-angled GBs is its major diagnosis in the GB map, which is somehow subjective (but see an attempt to quantify ruggedness in Choi et al. [2019: fig. S3]). More work needs to be done to refine this criterion for this type.

Identification of type II squamatic ultrastructure is less subjective in the GB map. We define it as areas with both rugged low- and high-angled GBs, in which the low-angled GBs are far more developed, intertwine, and form multiple, small scaly subgrains within the large grains formed by high-angled GBs (Fig. 6B). Good examples of this type in recent avian eggshell include the outer part of the squamatic zone of rhea (*Rhea* sp.), elephant bird (Aepyornithidae) eggshells, and the "thin and middle thickness moa eggshells" (Choi et al. 2023). Some fossil non-avian dinosaur eggshells also exhibit type II squamatic ultrastructure, including the whole continuous layer of *Elongatoolithus* sp. and most of the continuous layer of *Elongatoolithus subtitectorius* (Choi et al. 2022a) and *Macroelongatoolithus xixiaensis* (Choi et al. 2019). It is also the same for the outer sublayer of *R. acicularis* (Choi and Lee 2019), as long as it is not diagenetically altered too much.

The continuous layer of elongatoolithid eggshell is usually known to have type II squamatic ultrastructure. Our results show that the existence and distribution of type II squamatic ultrastructure are not the same in all examined oospecies, and type I squamatic ultrastructure may also occur in some. *Elongatoolithus elongatus* has type II squamatic ultrastructure throughout its continuous layer, while *Macroolithus yaotunensis* and *M. xixiaensis* also have type II squamatic ultrastructure in most parts of the continuous layer other than those places with prismatic grains, and these oospecies are also the most widely known elongatoolithid oospecies. Type II squamatic ultrastructure is far less developed in the continuous layer of the other four oogenera, which is reflected by the decrease of rugged low-angled GBs (Fig. 4C–F) and the rise of high-angled misorientations in the continuous layer (Supplementary Figs. 12C, 18C, 23B, 27B). The rugged low-angled GBs are scattered in the continuous layer of these eggshells rather than forming a network, so we interpret the continuous layer as having only type I squamatic ultrastructure.

It is interesting that type II squamatic ultrastructure seems to be absent in all Neognathae eggshells in literature, while it is developed in a small number of Mesozoic non-avian theropod eggshells and present in certain parts of the squamatic zones in some palaeognath eggshells (Table 1). Typical elongatoolithid eggshells such as *Elongatoolithus*, *Macroolithus*, and *Macroelongatoolithus* tend to have type II squamatic ultrastructure in almost the whole squamatic zone.

Figure 6. Diagrammatic sketches of two types of squamatic ultrastructure. A, Type I, rugged grain boundaries (GBs) are mostly high-angled; B, type II, rugged GBs are both high-angled and low-angled.

Ultrastructural Variation among Elongatoolithid Eggs

Oogenus- and oospecies-level classification of elongatoolithid eggshells has been focused on quantitative characters such as
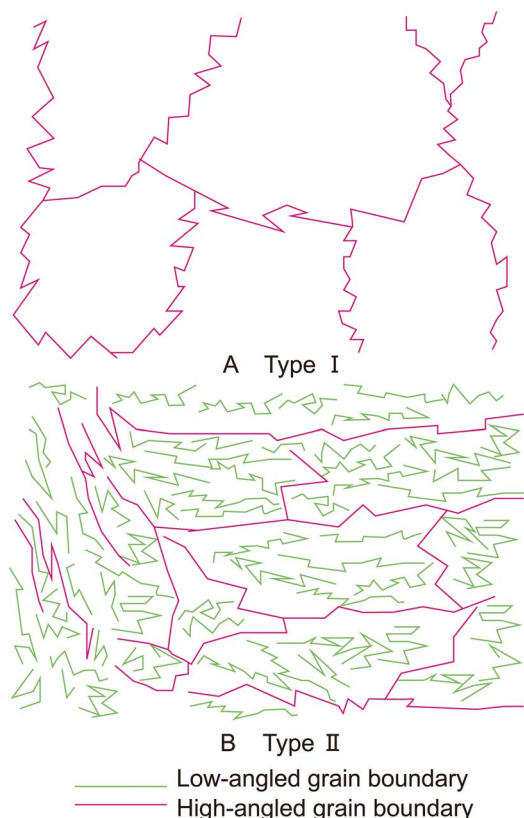
Table 1. List of eggshells in the literature that can be used to identify types of squamatic ultrastructure

Taxon or ootaxon		State of squamatic ultrastructure[a]	Reference
Mesozoic theropod eggshells			
	Elongatoolithus sp.	Whole SZ type II	Choi et al. 2019
	Elongatoolithus elongatus	Whole SZ type II	This study
	Elongatoolithus subtitectorius	SZ mostly type II	Choi et al. 2022a
	Macroolithus yaotunensis	SZ mostly type II	This study
	Macroelongatoolithus xixiaensis	SZ mostly type II	Choi et al. 2019; this study
	Undulatoolithus pengi	Whole SZ type I	This study
	Heishanoolithus changii	Whole SZ type I	This study
	Nanhsiungoolithus chuetienensis	Whole SZ type I	This study
	Paraelongatoolithus reticulatus	Whole SZ type I	This study
	Protoceratopsidovum sincerum	Whole SZ type I	Choi et al. 2022a
	Protoceratopsidovum fluxuosum	Whole SZ type I	Choi et al. 2022a
	Reticuloolithus acicularis	Inner SZ type I, outer SZ type II	Choi and Lee 2019
	Prismatoolithus levis	Whole SZ type I	Choi et al. 2019, 2022a
	Trigonoolithus amoae	Whole SZ type I	Moreno-Azanza et al. 2013, 2014
	Gobioolithus minor	Whole SZ type I	Choi et al. 2019
Cenozoic avian eggshells			
Palaeognathae	*Struthio camelus*	Whole SZ type I	Choi et al. 2023
	Dromaius novaehollandiae	Whole SZ type I	Choi et al. 2023
	Casuarius casuarius	Whole SZ type I	Choi et al. 2023
	Apteryx mantelli	Whole SZ type I	Choi et al. 2023
	Eudromia elegans	Whole SZ type I	Choi et al. 2023
	Nothoprocta perdicaria	Whole SZ type I	Choi et al. 2023
	"Thick moa eggshells"	Whole SZ type I	Choi et al. 2023
	Rhea sp.	Inner SZ type I, outer SZ type II	Choi et al. 2023
	Aepyornithidae	Inner SZ type I, outer SZ type II	Choi et al. 2023
	"Thin and middle thickness moa eggshells"	Inner SZ type I, outer SZ type II	Choi et al. 2023
	Lithornis vulturinus	Whole SZ type I	Grellet-Tinner and Dyke 2005; Choi et al. 2023
Neognathae	*Anas platyrhynchos domesticus*	Whole SZ type I	Choi et al. 2019
	Gallus gallus domesticus	Whole SZ type I	Choi et al. 2019
	Parus minor	Whole SZ type I	Choi et al. 2019
	Pica sericea	Whole SZ type I	Choi et al. 2019
	Alectura lathami	Probably whole SZ type I	Grellet-Tinner et al. 2017
	Leipoa ocellata	Probably whole SZ type I	Grellet-Tinner et al. 2017
	Phoenicopterus ruber	Probably whole SZ type I	Grellet-Tinner et al. 2012
	Phoenicopteridae	Probably whole SZ type I	Grellet-Tinner et al. 2012

[a]SZ, squamatic zone.

eggshell thickness and the ratio of layers or some non-quantitative characters like ornamentation that can be categorized (Mikhailov 1997b; Tanaka et al. 2011). The microstructural variation in elongatoolithids has been relatively unexplored.

Although all could be classified as calcite radial ultrastructure (Mikhailov 1997b), the mammillary structures of the oospecies studied in this work are not the same. The mammillae of *E. elongatus*, *M. yaotunensis*, *Heishanoolithus changii*, *Undulatoolithus pengi*, and *M. xixiaensis* (Fig. 7A–D,G) are compactly arranged within the mammillary layer and can hardly be separated from each other, while each mammilla is composed of radiating wedges. On the contrary, the mammillae of *P. reticulatus* and *Nanhsiungoolithus chuetienensis* (Fig. 7E,F) are more loosely arranged and the calcite wedges that constitute a mammilla are more slender than those in mammillae of former oospecies, which in morphology are similar to the acicular structures
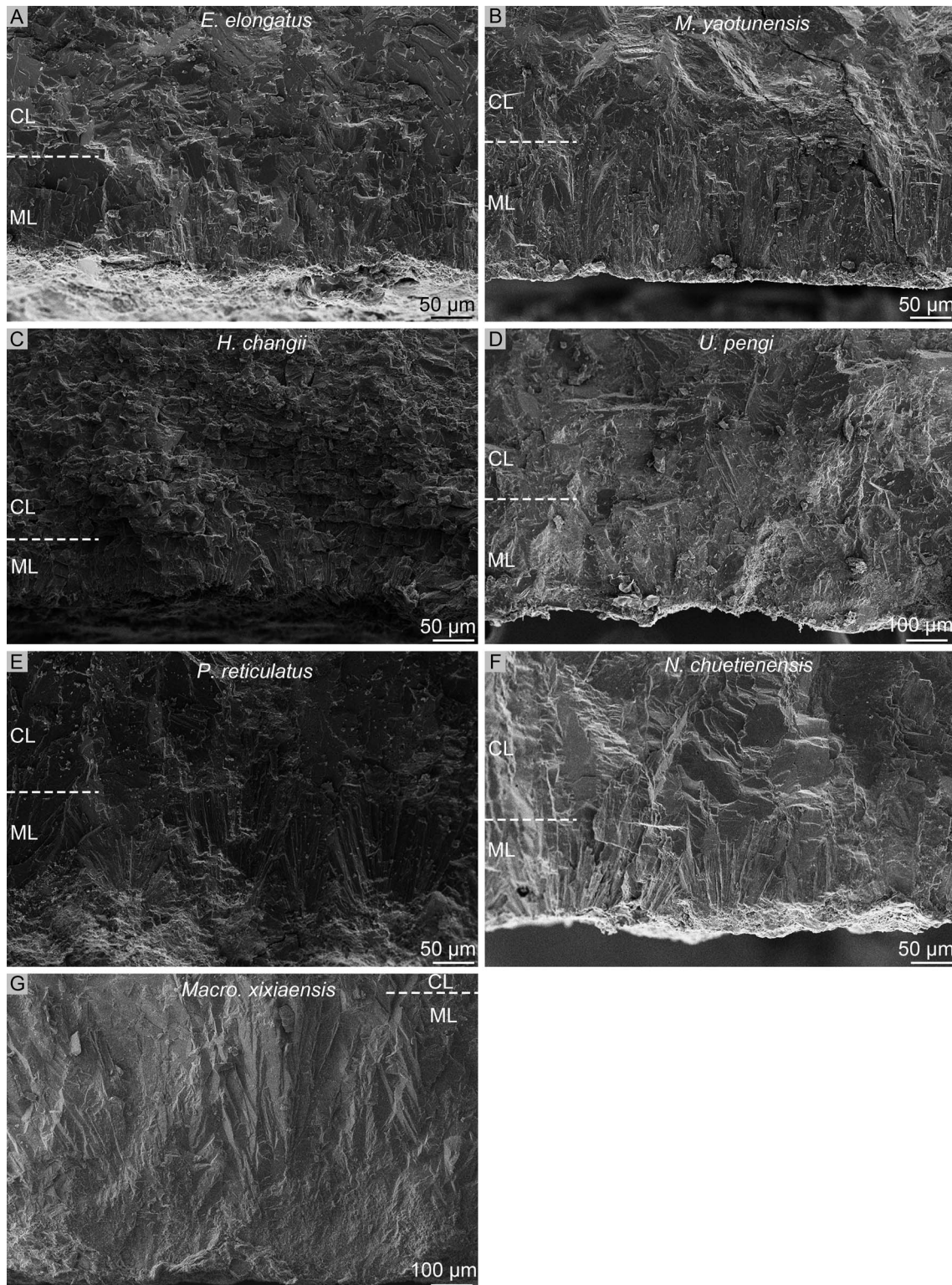
Figure 7. Mammillary structures of the eggshells. A, *Elongatoolithus elongatus* (IVPP V 734); B, *Macroolithus yaotunensis* (IVPP V 2781); C, *Heishanoolithus changii* (IVPP V 11578); D, *Undulatoolithus pengi* (PXM V 0016); E, *Paraelongatoolithus reticulatus* (IVPP V 16514); F, *Nanhsiungoolithus chuetienensis* (IVPP V 2783); G, *Macroelongatoolithus xixiaensis* (TTM 15). CL, continuous layer; ML, mammillary layer.

described by other researchers (Grellet-Tinner and Makovicky 2006; Choi and Lee 2019; Choi et al. 2019). The difference in mammillary morphology has already been mentioned by former researchers and could also be used to describe the mammillary

morphology of some other theropod eggshells (Tanaka et al. 2016). The slender calcite wedges in the mammilla of *N. chuetienensis* and *P. reticulatus* are not constant in width (e.g., in *P. reticulatus*, the width of the wedges in the mammillae

ranges from 5–8 μm near the inner surface to about 25 μm near the continuous layer; Fig. 4E). The difference between acicular and wedged mammillae might simply result from different areal density of organic cores on the shell membrane.

So far, we have observed that, aside from scaly calcite subgrains consisting of type II squamatic ultrastructure, there are at least two additional morphological types of calcite grains in the continuous layer of elongatoolithid eggshells. One type is usually columnar, prismatic, or wedge-shaped and can exist in multiple places in the continuous layer. It could appear as several columns at the central base of the ridges of *M. yaotunensis* (type B; Fig. 4B) and columns or wedges in the continuous layer of *P. reticulatus* (Fig. 4E) and *N. chuetienensis* (Fig. 4F). These grains are relatively large and separated from each other by high-angled GBs and lack low-angled GBs within them. The other type is characterized by radially arranged slender calcite subgrains that are separated by straight, extending low-angled GBs, which are similar to the radiating subgrains in eggshells possessing spherulitic eggshell units (Grellet-Tinner et al. 2011; Trimby and Grellet-Tinner 2011; Moreno-Azanza et al. 2013, 2016, 2017; Eagle et al. 2015), therefore lacking squamatic ultrastructure. This type often appears right beneath the ornamentations, and it seems possible that the oospecies with relative prominent ridges tend to show this type, as in *M. yaotunensis, U. pengi* (Fig. 4B,D), and *M. xixiaensis* (Choi et al. 2019: fig. 4B), which explains the decrease of squamatic ultrastructure in calcite grains that constitute the ornamentation (Choi et al. 2019).

In *M. yaotuneinsis*, all three morphological types of calcite grains can be observed within a proper radial thin section that crosses the middle part of a prominent ridge (Supplementary Fig. 5). On the other hand, it could be possible that only scaly subgrains indicating type II squamatic ultrastructure can be observed because the thin sections cross the region between the ridges or eggshells with low ridges (usually those from the very end of the polar region). It is also possible that the calcite grains of the continuous layer might exhibit a different way in another part of the egg or in a section with different angle crossing the eggshell, neither of which occurs in this sample; this would require thorough study in the future.

Historically, the microstructure of *M. yaotunensis* was not highly appreciated; the variation of calcite grains in its continuous layer was unknown because of the lack of EBSD study. However, structures reflecting different calcite grain morphology in *Macroolithus* can be seen in some old work. For example, the columns beneath ornamentations can be seen as structures that jack up accretion lines in many published photographs of *M. yaotunensis* (Cheng et al. 2008; Wang et al. 2016). Some early published sketches of elongatoolithid eggshells also reflected this structure by illustrating the presence of jacked-up accretion lines near the ridges (Sochava 1969: fig. 2A; Sabath 1991; Mikhailov 1994: figs. 7.2I, 7.13C), but provided little description. A continuous layer with similar structure can also be seen in another oospecies of *Macroolithus, M. rugustus*, which is diagnostically different from *M. yaotunensis* mainly in the non-undulating boundary between the mammillary and continuous layers (Zhao 1975). The third oospecies of *Macroolithus, M. mutabilis*, is known only from pictures of fragments (Mikhailov 1994); therefore, we cannot be sure that the continuous layer of its eggshell is also similar. Should all *Macroolithus* oospecies have the same combination of calcite morphology in the continuous layer, this would be a good auxiliary diagnostic characteristic for this oogenus, as the major microstructural diagnosis of *Macroolithus*, the distinct

boundary between the mammillary and continuous layers, can be easily modified by diagenesis (Wang et al. 2016: fig. 4B; Bi et al. 2021: fig. 2B), but the combination of accretion lines jacked up by calcite columns below the ridges and the radiating calcite subgrains that show sweeping extinction could be more preservable and recognizable in the same specimen (Wang et al. 2016: fig. 4B).

Same combination of the three grain types can also be observed in *Macroelongatoolithus*. Choi et al. (2019) reported that the squamatic ultrastructure decreases in the calcite grains that constitute the ornamentation of *Macroelongatoolithus*, which in our view is similar to what happens in *Macroolithus*, as those grains became more prismatic under ornamentation and those radially arranged subgrains near the outer surface (Choi et al. 2019: fig. 4B) are remarkably similar to the second and third types of calcite grains in *Macroolithus* in shape, GB characters, and distributions. Jin et al. (2007) observed the prismatic columns in the continuous layer of *Macroelongatoolithus*, which it is primarily or completely concealed by squamatic ultrastructure, and described this as "cryptoprismatic." We find these cryptoprismatic columns similar to the type B calcite grains in *Macroolithus*, whose grain boundaries also seems linear (Jin et al. 2007: fig. 2E).

Suggested Parataxonomic Revision of Paraelongatoolithus and Nanhsiungoolithus

Zelenitsky and Sloboda (2005) erected *Reticuloolithus hirschi* based on eggshell fragments from southern Alberta and Montana, which have reticulated ornamentation and two-layered microstructure with acicular mammillae. The second oospecies of *Reticuloolithus, R. acicularis*, was named by Choi and Lee (2019) based on eggshell having a similar structure from the Upper Cretaceous of Wi Island, South Korea. These two ootaxa have been proposed to be produced by dromaeosaurs, because a specimen preserving a partial egg in contact with articulated gastralia of *Deinonychus antirrhopus* was described by Grellet-Tinner and Makovicky (2006), and its eggshell has macro- and microstructures similar to those of *R. hirschi*. In the meantime, the eggshell related to *D. antirrhopus* was assigned to *P. reticulatus* by Wang et al. (2010a), who erected this oospecies based on a partial egg that was excavated from the Upper Cretaceous Chichengshan Formation of the Tiantai Basin, Zhejiang Province, China. Choi and Lee (2019) suggested that *Paraelongatoolithus* could be a synonym of *Reticuloolithus* if the mammilla of *Paraelongatoolithus* is also acicular. Although our EBSD (Fig. 4E) and SEM (Fig. 7E) results show one well-preserved mammilla that has the same acicular structure as *Reticuloolithus* in *P. reticulatus*, which would support the close relationship between *Paraelongatoolithus* and *Reticuloolithus*, the structure in the continuous layer of *P. reticulatus* is different from what is described in *R. acicularis* and the eggshell related to *Deinonychus*. The *Deinonychus* eggshell was described as having slightly different structure between the lower and the upper part of its continuous layer (Grellet-Tinner and Makovicky 2006). Choi and Lee (2019) also identified two sublayers in the continuous layer of the *R. acicularis* eggshell and suggested the possible homology between the *R. acicularis* and *Deinonychus* eggshells. They also claimed that squamatic ultrastructure exists in the continuous layer of *R. acicularis*, which we classified as type I squamatic ultrastructure (see the first section in the "Discussion"). On the other hand, the basically non-diagenetic continuous layer of *P. reticulatus* eggshell is

composed of a single layer of wedges that are separated by nearly vertically extended high-angled GBs with a few low-angled ones. This may also represent the presence of type I squamatic ultrastructure and is similar to the inner sublayer of *R. acicularis*, although there is no trace of an outer sublayer that has type II squamatic ultrastructure. One explanation is that a possible outer sublayer in the continuous layer of *P. reticulatus* specimen is eroded and not preserved, which is supported by its reduced thickness and discontinuity of accretion lines near the outer surface in the radial section (Supplementary Fig. 20A). A specimen identified as *P. sincerum* (PIN 3143/121; Choi et al. 2022a: figs. 3, 9) is very similar to *Paraelongatoolithus* in its acicular mammillae (although they seem to be more compact than those in either *Paraelongatoolithus* or *Reticuloolithus*), abrupt boundary between structural layers, and columnar continuous layer, although its outer surface is severely eroded and hinders observation of its ornamentation. Therefore, before future synonymization of these oogenera, the existence of an outer sublayer would have to be solved first by examination on more well-preserved specimens. Currently, based on the reticulated ornamentation, a continuous layer that shows columnar extinction, and acicular mammillae, this study suggests this oogenera ought to be placed outside the oofamily Elongatoolithidae, as these characters differ from those of the typical elongatoolithid oogenera like *Elongatoolithus* and are not consistent with the diagnosis of Elongatoolithidae.

Similar to *Paraelongatoolithus*, *Nanhsiungoolithus* has a continuous layer that shows columnar extinction (Supplementary Fig. 24B) and acicular mammillae (Supplementary Fig. 24C), but its surface ornamentation is not very prominent. Zhao (1975) described its outer surface as smooth or having faint ridges, which is also our observation. The oofamily Montanoolithidae shares columnar extinction with *Nanhsiungoolithus*, but has reticulated or anastomosing ornamentation (Zelenitsky and Therrien 2008: fig. 3) and a much more compact mammillary layer (Zelenitsky and Therrien 2008: fig. 4A; Vila et al. 2017: fig. 2B) similar to that in *Macroolithus*. If a better preserved specimen of *Nanhsiungoolithus* shows reticulated or anastomosing ornamentation, it would be a good reason to move this oogenus out of Elongatoolithidae, just like *Paraelongatoolithus*.

Abnormal Eggshell Structure in Undulatoolithus

Biological abnormality in the microstructure of eggshells is not rare in eggs of both recent and fossil species. Female birds that ingest synthetic pesticides through the food chain could produce significantly thinner or even soft eggshells (Hickey and Anderson 1968; Oestreicher et al. 1971; Lincer 1975; Pruett-Jones et al. 1981; Lundholm 1997; Holm et al. 2006; Bouwman et al. 2019). Delayed oviposition derived by environmental stresses can cause the formation of multilayered eggshells in birds, non-avian dinosaurs, and turtles (Romanoff and Romanoff 1949; Ewert et al. 1984; Jackson and Varricchio 2003; Jackson et al. 2004; Sellés et al. 2017; Bailleul et al. 2019). Other disorders of the avian female reproductive system related to abnormal eggshell and rarely seen microstructural abnormalities in non-avian dinosaur eggshells have also been reported, most of which are related to aging or infection of the female birds (Romanoff and Romanoff 1949; Keymer 1980; Grellet-Tinner et al. 2010).

In the eggshell of *U. pengi*, this study identified an abnormal layer additional to the outside of the normal eggshell. At some places, this layer seems to grow from a series of nucleation centers (Supplementary Fig. 14F), while at most places, there are no nucleation centers, and the grains maintain the orientation of the calcite grains beneath this layer (Fig. 3D, Supplementary Fig. 14E). The two conditions of the additional layer of *U. pengi* are similar to type I and II abnormality (sensu Jackson et al. 2004) reported in titanosaur eggshells, respectively (Jackson et al. 2004; Jackson and Schmitt 2008). Delayed oviposition as a stress response to external stimuli would be the best explanation for this abnormal structure.

Undulatoolithus pengi is known from the only clutch (PXMV-0016) consisting of four pairs of eggs (Wang et al. 2013). While the abnormal layer can be clearly seen in multiple samples from egg no. 6 from the clutch, it is absent in the other five eggs sampled (Supplementary Fig. 19), suggesting the abnormal nature of this layer. Further research may be carried out on its significance for dinosaur breeding behavior.

Identification of an External Zone in Heishanoolithus

The external zone is commonly seen in the eggshells of modern birds and is regarded as an ultrastructural zone in the outermost part of the continuous layer, which under chemical treatment would exhibit clear vertical boundaries of columnar or prismatic calcite grains (Mikhailov 1997b). Tyler (1965) cited this structure as the surface crystal layer and treated it as an independent third layer outside the continuous layer. The external zone has been reported in troodontid eggshells (Prismatoolithidae) like *P. levis* (eggs of *Troodon formosus*; Varricchio and Jackson 2004), as the GBs in its continuous layer become more linear near the outer surface (Choi et al. 2019). Moreno-Azanza et al. (2014) reported an external layer in the eggshell of *T. amoae* (Prismatoolithidae), which appears as a layer of coarse prismatic crystal. However, the prisms are nearly euhedral or subhedral based on their triangular "nodes" on the outer surface (Canudo et al. 2010: fig. 6-4; Moreno-Azanza et al. 2014: fig. 2A), suggesting that it might be formed by recrystallization. *Arriagadoolithus patagoniensis* (eggs preserved with an alvarezsaurid theropod) is also reported to have an external layer (Agnolin et al. 2012), although we believe the silicon-rich secondary matrix between its "external layer" and the prismatic layer (Agnolin et al. 2012: fig. 10B,G) suggest that this external layer is probably a layer of secondary calcite. The eggshell of *Triprismatoolithus stephensi* is reported to have an external layer (Jackson and Varricchio 2010).

In elongatoolithid eggs, the existence of an external zone has never been confirmed. Our EBSD result shows the eggshell of *H. changii* exhibits a continuous layer that has a typical squamatic ultrastructure in its inner part as the squamatic zone and an overlying zone of prismatic calcite grains (Fig. 4C). The prisms in this zone are separated by vertical GBs that extend linearly, which in morphology suits the definition of an external zone. It is important that the squamatic zone and this zone can even be easily differentiated through a radial thin section with cross-polarized light by the contrast of irregular extinction below and prismatic extinction near the surface (Supplementary Fig. 9B). The accretion lines are more prominent in the external zone of *H. changii*, which testifies to the biogenic origin of this structure. Parataxonomically, the presence of an external zone in *H. changii* does not suit the diagnosis of Elongatoolithidae, which lacks an external zone (Zhao 1975; Mikhailov 1997b). We hereby suggest removing *Heishanoolithus* from the oofamily Elongatoolithidae.

A North American oospecies, *Continoolithus canadensis* (Zelenitsky et al. 1996) caught our attention when we noted

that the same combination of the irregular extinction in its inner part and the prismatic extinction near the outer surface is shown in a thin-section micro-photograph showing its extinction pattern (Jackson and Varricchio 2010: fig. 8). The accretion lines also became more prominent near the outer one-fifth of the eggshell. Therefore, we find it possible that the eggshell of *C. canadensis*, which was described as having two structural layers, also has an external zone that is similar to that of *H. changii*. Also, the thickness, layer ratio, and mammillary shapes of the two oospecies are similar, and the ornamentation types are both dispersituberculate, which suggests a close relationship between them.

Taxonomic Affinity of Elongatoolithid Eggs

The relationship between elongatoolithid eggs and oviraptorosaurs have been widely known due to the discovery of skeleton–egg associations (Norell et al. 1995; Dong and Currie 1996; Clark et al. 1999; Sato et al. 2005; Fanti et al. 2012; Pu et al. 2017; Jin et al. 2020; Bi et al. 2021) and eggs containing embryos (Norell et al. 1994; Cheng et al. 2008; Weishampel et al. 2008; Shao et al. 2014; Wang et al. 2016; Xing et al. 2022). These cases involve only three oogenera, *Elongatoolithus*, *Macroolithus*, and *Macroelongatoolithus*. However, this study shows *Heishanoolithus* and *Paraelongatoolithus* should no longer be regarded as members of Elongatoolithidae, and *Nanhsiungoolithus* may also be a oogenus outside Elongatoolithidae, and these ootaxa are likely to be produced by other theropod dinosaurs such as dromaeosaurs. Although possible, it is uncertain that other oogenera are also produced by oviraptorosaurs. Therefore, the relationship between elongatoolithid eggs and oviraptorosaurs should not be exclusively extended to all members of this group.

Conclusion

The EBSD technique provides a method to objectively distinguish microstructural differences in eggshells. Our results have revealed more structural information in elongatoolithid eggshells. We have shown that the structure of elongatoolithid eggshells is more diverse than traditionally thought, even in oospecies that are widely known like *Macroolithus*. The newly identified external zone makes *Heishanoolithus* no longer suitable as a member of the oofamily Elongatoolithidae. The combination of reticulated ornamentation, a continuous layer that shows columnar extinction, and acicular mammillae suggests that *Paraelongatoolithus* is not a member of Elongatoolithidae. We also discussed the variation of squamatic ultrastructure in fossil and recent eggshells and proposed practical criteria to distinguish them into two types. These findings may prove to be useful in the future classification of fossil eggshells and discussion about their producers and will help us in understanding the evolution and adaption of fossil and recent eggshells.

Literature Cited

Agnolin, F. L., J. E. Powell, F. E. Novas, and M. Kundrát. 2012. New alvarezsaurid (Dinosauria, Theropoda) from uppermost Cretaceous of northwestern Patagonia with associated eggs. *Cretaceous Research* **35**:33–56.

Bailleul, A. M., J. O'Connor, S. Zhang, Z. Li, Q. Wang, M. C. Lamanna, X. Zhu, and Z. Zhou. 2019. An Early Cretaceous enantiornithine (Aves) preserving an unlaid egg and probable medullary bone. *Nature Communications* **10**:1275.

Bi, S., R. Amiot, C. Peyre de Fabrègues, M. Pittman, M. C. Lamanna, Y. Yu, C. Yu, *et al.* 2021. An oviraptorid preserved atop an embryo-bearing egg clutch sheds light on the reproductive biology of non-avialan theropod dinosaurs. *Science Bulletin* **66**:947–954.

Bouwman, H., Y. B. Yohannes, S. M. M. Nakayama, K. Motohira, M. Ishizuka, M. S. Humphries, V. van der Schyff, M. du Preez, A. Dinkelmann, and Y. Ikenaka. 2019. Evidence of impacts from DDT in pelican, cormorant, stork, and egret eggs from KwaZulu-Natal, South Africa. *Chemosphere* **225**:647–658.

Canudo, J. I., J. M. Gasca, M. Aurell, A. Badiola, H.-A. Blain, P. Cruzado-Caballero, D. Gomez-Fernández, *et al.* 2010. La Cantalera: an exceptional window onto the vertebrate biodiversity of the Hauterivian–Barremian transition in the Iberian Peninsula. *Journal of Iberian Geology* **36**:205–224.

Cheng, Y., Q. Ji, X. Wu, and H. Shan. 2008. Oviraptorosaurian eggs (Dinosauria) with embryonic skeletons discovered for the first time in China. *Acta Geologica Sinica—English Edition* **82**:1089–1094.

Choi, S. 2020. Paleontological, neontological, and taphonomic studies for amniote eggshells with analytical approaches. Seoul National University, Seoul.

Choi, S., and Y.-N. Lee. 2019. Possible Late Cretaceous dromaeosaurid eggshells from South Korea: a new insight into dromaeosaurid oology. *Cretaceous Research* **103**:104167.

Choi, S., S. Han, N.-H. Kim, and Y.-N. Lee. 2018. A comparative study of eggshells of Gekkota with morphological, chemical compositional and crystallographic approaches and its evolutionary implications. *PLoS ONE* **13**: e0199496.

Choi, S., S. Han, and Y.-N. Lee. 2019. Electron backscatter diffraction (EBSD) analysis of maniraptoran eggshells with important implications for microstructural and taphonomic interpretations. *Palaeontology* **62**:777–803.

Choi, S., D. E. Barta, M. Moreno-Azanza, N. Kim, C. A. Shaw, and D. J. Varricchio. 2022a. Microstructural description of the maniraptoran egg *Protoceratopsidovum*. *Papers in Palaeontology* **8**:e1430.

Choi, S., H. Kim, I. Paik, Y. Park, H. Jung, and X. Xu. 2022b. Turtle eggs from the Lower Cretaceous Hasandong Formation (South Korea) with relict aragonite under significant thermal maturity. *Journal of Vertebrate Paleontology* **42**:e2183866.

Choi, S., N.-H. Kim, H.-I. Kim, J. J. Kweon, S. K. Lee, S. Zhang, and D. J. Varricchio. 2022c. Preservation of aragonite in Late Cretaceous (Campanian) turtle eggshell. *Palaeogeography, Palaeoclimatology, Palaeoecology* **585**:110741.

Choi, S., M. E. Hauber, L. J. Legendre, N.-H. Kim, Y.-N. Lee, and D. J. Varricchio. 2023. Microstructural and crystallographic evolution of palaeognath (Aves) eggshells. *eLife* **12**:e81092.

Clark, J. M., I. M. A. Norell, and L. M. Chiappe. 1999. An oviraptorid skeleton from the Late Cretaceous of Ukhaa Tolgod, Mongolia, preserved in an avianlike brooding position over an oviraptorid nest. *American Museum Novitates* **3265**:1–36.

Cusack, M. 2016. Biomineral electron backscatter diffraction for palaeontology. *Palaeontology* **59**:171–179.

Cusack, M., Y. Dauphin, P. Chung, A. Pérez-Huerta, and J.-P. Cuif. 2008a. Multiscale structure of calcite fibres of the shell of the brachiopod *Terebratulina retusa*. *Journal of Structural Biology* **164**:96–100.

Cusack, M., J. England, P. Dalbeck, A. W. Tudhope, A. E. Fallick, and N. Allison. 2008b. Electron backscatter diffraction (EBSD) as a tool for detection of coral diagenesis. *Coral Reefs* **27**:905–911.

Dalbeck, P., and M. Cusack. 2006. Crystallography (electron backscatter diffraction) and chemistry (electron probe microanalysis) of the avian eggshell. *Crystal Growth & Design* **6**:2558–2562.

Dauphin, Y., G. Luquet, A. Perez-Huerta, and M. Salomé. 2018. Biomineralization in modern avian calcified eggshells: similarity versus diversity. *Connective Tissue Research* 59:67–73.

Dong, Z.-M., and P. J. Currie. 1996. On the discovery of an oviraptorid skeleton on a nest of eggs at Bayan Mandahu, Inner Mongolia, People's Republic of China. *Canadian Journal of Earth Sciences* 33:631–636.

Eagle, R. A., M. Enriquez, G. Grellet-Tinner, A. Pérez-Huerta, D. Hu, T. Tütken, S. Montanari, et al. 2015. Isotopic ordering in eggshells reflects body temperatures and suggests differing thermophysiology in two Cretaceous dinosaurs. *Nature Communications* 6:8296.

Ewert, M. A., S. J. Firth, and C. E. Nelson. 1984. Normal and multiple eggshells in batagurine turtles and their implications for dinosaurs and other reptiles. *Canadian Journal of Zoology* 62:1834–1841.

Fanti, F., P. J. Currie, and D. Badamgarav. 2012. New specimens of Nemegtomaia from the Baruungoyot and Nemegt Formations (Late Cretaceous) of Mongolia. *PLoS ONE* 7:e31330.

Grellet-Tinner, G., and G. J. Dyke. 2005. The eggshell of the Eocene bird *Lithornis*. *Acta Palaeontologica Polonica* 50:831–835.

Grellet-Tinner, G., and P. Makovicky. 2006. A possible egg of the dromaeosaur *Deinonychus antirrhopus*: phylogenetic and biological implications. *Canadian Journal of Earth Sciences* 43:705–719.

Grellet-Tinner, G., F. Corsetti, and A. D. Buscalioni. 2010. The importance of microscopic examinations of eggshells: Discrimination of bioalteration and diagenetic overprints from biological features. *Journal of Iberian Geology* 36:181–192.

Grellet-Tinner, G., C. M. Sim, D. H. Kim, P. Trimby, A. Higa, S. L. An, H. S. Oh, T. Kim, and N. Kardjilov. 2011. Description of the first lithostrotian titanosaur embryo in ovo with neutron characterization and implications for lithostrotian Aptian migration and dispersal. *Gondwana Research* 20:621–629.

Grellet-Tinner, G., X. Murelaga, J. C. Larrasoaña, L. F. Silveira, M. Olivares, L. A. Ortega, P. W. Trimby, and A. Pascual. 2012. The first occurrence in the fossil record of an aquatic avian twig-nest with Phoenicopteriformes eggs: evolutionary implications. *PLoS ONE* 7:e46972.

Grellet-Tinner, G., N. A. Spooner, and T. H. Worthy. 2016. Is the "Genyornis" egg of a mihirung or another extinct bird from the Australian dreamtime? *Quaternary Science Reviews* 133:147–164.

Grellet-Tinner, G., S. Lindsay, and M. Thompson. 2017. The biomechanical, chemical, and physiological adaptations of the eggs of two Australian megapodes to their nesting strategies and their implications for extinct titanosaur dinosaurs. *Journal of Microscopy* 267:237–246.

Han, F., Y. Yu, S. Zhang, R. Zeng, X. Wang, H. Cai, T. Wu, et al. 2023. Exceptional early Jurassic fossils with leathery eggs shed light on dinosaur reproductive biology. *National Science Review* 11:nwad258.

Hickey, J. J., and D. W. Anderson. 1968. Chlorinated hydrocarbons and eggshell changes in raptorial and fish-eating birds. *Science* 162:271–273.

Holm, L., A. Blomqvist, I. Brandt, B. Brunström, Y. Ridderstråle, and C. Berg. 2006. Embryonic exposure to o,p′-DDT causes eggshell thinning and altered shell gland carbonic anhydrase expression in the domestic hen. *Environmental Toxicology and Chemistry* 25:2787–2793.

Jackson, F. D., and J. G. Schmitt. 2008. Recognition of vertebrate egg abnormalities in the Upper Cretaceous fossil record. *Cretaceous Research* 29:27–39.

Jackson, F. D., and D. J. Varricchio. 2003. Abnormal, multilayered eggshell in birds: implications for dinosaur reproductive anatomy. *Journal of Vertebrate Paleontology* 23:699–702.

Jackson, F. D., and D. J. Varricchio. 2010. Fossil eggs and eggshell from the lowermost Two Medicine Formation of western Montana, Sevenmile Hill locality. *Journal of Vertebrate Paleontology* 30:1142–1156.

Jackson, F. D., A. Garrido, J. G. Schmitt, L. M. Chiappe, L. Dingus, and D. B. Loope. 2004. Abnormal, multilayered titanosaur (Dinosauria: Sauropoda) eggs from in situ clutches at the Auca Mahuevo locality, Neuquén Province, Argentina. *Journal of Vertebrate Paleontology* 24:913–922.

Jain, S., S. Bajpai, G. Kumar, and V. Pruthi. 2016. Microstructure, crystallography and diagenetic alteration in fossil ostrich eggshells from Upper Palaeolithic sites of Indian peninsular region. *Micron* 84:72–78.

Jin, X., D. J. Varricchio, A. W. Poust, and T. He. 2020. An oviraptorosaur adult–egg association from the Cretaceous of Jiangxi Province, China. *Journal of Vertebrate Paleontology* 39:e1739060.

Jin, X. S., Y. Azuma, F. D. Jackson, and D. J. Varricchio. 2007. Giant dinosaur eggs from the Tiantai basin, Zhejiang Province, China. *Canadian Journal of Earth Sciences* 44:81–88.

Keymer, I. F. 1980. Disorders of the avian female reproductive system. *Avian Pathology* 9:405–419.

Kim, N.-H., S. Choi, S. Kim, and Y.-N. Lee. 2019. A new faveoloolithid oogenus from the Wido Volcanics (Upper Cretaceous), South Korea and a new insight into the oofamily Faveoloolithidae. *Cretaceous Research* 100:145–163.

Lincer, J. L. 1975. DDE-induced eggshell-thinning in the American kestrel: a comparison of the field situation and laboratory results. *Journal of Applied Ecology* 12:781.

Lundholm, C. E. 1997. DDE-induced eggshell thinning in birds: Effects of p, p′-DDE on the calcium and prostaglandin metabolism of the eggshell gland. *Comparative Biochemistry and Physiology Part C: Pharmacology, Toxicology and Endocrinology* 118:113–128.

Mikhailov, K. E. 1991. Classification of fossil eggshells of amniotic vertebrates. *Acta Palaeontologica Polonica* 36:193–238.

Mikhailov, K. E. 1994. Theropod and protoceratopsian dinosaur eggs from the Cretaceous of Mongolia and Kazakhstan. *Paleontological Journal* 28:101–120.

Mikhailov, K. E. 1997a. *Avian eggshells: an atlas of scanning electron micrographs*. British Ornithologists' Club, Tring.

Mikhailov, K. E. 1997b. Fossil and recent eggshell in amniotic vertebrates: fine structure, comparative morphology and classification. *Special Papers in Palaeontology* 56:1–80.

Mikhailov, K. E. 2014. Eggshell structure, parataxonomy and phylogenetic analysis: some notes on articles published from 2002 to 2011. *Historical Biology* 26:144–154.

Mikhailov, K. E. 2019. Conservative nature of biomineral structures as a challenge for the cladistic method of phylogeny reconstruction (illustrated by two groups of dinosaur eggs). *Paleontological Journal* 53:551–565.

Moreno-Azanza, M., E. Mariani, B. Bauluz, and J. I. Canudo. 2013. Growth mechanisms in dinosaur eggshells: an insight from electron backscatter diffraction. *Journal of Vertebrate Paleontology* 33:121–130.

Moreno-Azanza, M., J. I. Canudo, and J. M. Gasca. 2014. Unusual theropod eggshells from the Early Cretaceous Blesa Formation of the Iberian Range, Spain. *Acta Palaeontologica Polonica* 59:843–854.

Moreno-Azanza, M., B. Bauluz, J. I. Canudo, J. M. Gasca, and F. Torcida Fernández-Baldor. 2016. Combined use of electron and light microscopy techniques reveals false secondary shell units in Megaloolithidae eggshells. *PLoS ONE* 11:e0153026.

Moreno-Azanza, M., B. Bauluz, J. I. Canudo, and O. Mateus. 2017. The conservative structure of the ornithopod eggshell: electron backscatter diffraction characterization of *Guegoolithus turolensis* from the Early Cretaceous of Spain. *Journal of Iberian Geology* 43:235–243.

Moreno-Azanza, M., E. Díaz-Berenguer, R. Silva-Casal, A. Pérez-García, A. Badiola, and J. I. Canudo. 2021. Recognizing a lost nesting ground: First unambiguous Testudines eggshells from the Eocene, associated with the pleurodiran Eocenochelus (Huesca, Northern Spain). *Palaeogeography, Palaeoclimatology, Palaeoecology* 576:110526.

Norell, M. A., J. M. Clark, D. Demberelyin, B. Rhinchen, L. M. Chiappe, A. R. Davidson, M. C. McKenna, P. Altangerel, and M. J. Novacek. 1994. A theropod dinosaur embryo and the affinities of the flaming cliffs dinosaur eggs. *Science* 266:779–782.

Norell, I. M. A., J. M. Clark, L. M. Chiappe, and D. Dashzeveg. 1995. A nesting dinosaur. *Nature* 378:774–776.

Oestreicher, M. I., D. H. Shuman, and C. F. Wurster. 1971. DDE reduces medullary bone formation in birds. *Nature* 229:571–571.

Oser, S. E., K. Chin, J. J. W. Sertich, D. J. Varricchio, S. Choi, and J. Rifkin. 2021. Tiny, ornamented eggs and eggshell from the Upper Cretaceous of Utah represent a new ootaxon with theropod affinities. *Scientific Reports* 11:10021.

Pérez-Huerta, A., and M. Cusack. 2009. Optimizing electron backscatter diffraction of carbonate biominerals—resin type and carbon coating. *Microscopy and Microanalysis* **15**:197–203.

Pérez-Huerta, A., and Y. Dauphin. 2016. Comparison of the structure, crystallography and composition of eggshells of the guinea fowl and graylag goose. *Zoology* **119**:52–63.

Pérez-Huerta, A., Y. Dauphin, J. P. Cuif, and M. Cusack. 2011. High resolution electron backscatter diffraction (EBSD) data from calcite biominerals in recent gastropod shells. *Micron* **42**:246–251.

Prior, D. J., E. Mariani, and J. Wheeler. 2009. EBSD in the earth sciences: applications, common practice, and challenges. Pp. 345–360 *in* A. J. Schwartz, M. Kumar, B. L. Adams, and D. P. Field, eds. *Electron backscatter diffraction in materials science*. Springer US, Boston.

Pruett-Jones, S. G., C. M. White, and W. B. Emison. 1981. Eggshell thinning and organochlorine residues in eggs and prey of peregrine falcons from Victoria, Australia. *Emu—Austral Ornithology* **80**:281–287.

Pu, H., D. K. Zelenitsky, J. Lü, P. J. Currie, K. Carpenter, L. Xu, E. B. Koppelhus, *et al.* 2017. Perinate and eggs of a giant caenagnathid dinosaur from the Late Cretaceous of central China. *Nature Communications* **8**:14952.

Romanoff, A. L., and A. J. Romanoff. 1949. *The avian egg*. Wiley, New York.

Sabath, K. 1991. Upper Cretaceous amniotic eggs from Gobi Desert. *Acta Palaeontologica Polonica* **36**:151–192.

Sato, T., Y.-N. Cheng, X. Wu, D. K. Zelenitsky, and Y. Hsiao. 2005. A pair of shelled eggs inside a female dinosaur. *Science* **308**:375–375.

Schwarzer, R. A., D. P. Field, B. L. Adams, M. Kumar, and A. J. Schwartz. 2009. Present state of electron backscatter diffraction and prospective developments. Pp. 1–20 *in* A. J. Schwartz, M. Kumar, B. L. Adams, and D. P. Field, eds. *Electron backscatter diffraction in materials science*. Springer US, Boston.

Sellés, A. G., B. Vila, and À. Galobart. 2017. Evidence of reproductive stress in titanosaurian sauropods triggered by an increase in ecological competition. *Scientific Reports* **7**:13827.

Shao, Z., S. Fan, S. Jia, K. Tanaka, and J. Lü. 2014. Intact theropod dinosaur eggs with embryonic remains from the Late Cretaceous of southern China. *Geological Bulletin of China* **33**:941–948.

Sochava, A. V. 1969. Dinosaur eggs from the Upper Cretaceous of the Gobi Desert. *Paleontological Journal* **4**:517–527.

Tanaka, K., J. Lv, Y. Kobayashi, D. K. Zelenitsky, L. Xu, S. Jia, S. Qing, and M. Tang. 2011. Description and phylogenetic position of dinosaur eggshells from the Luanchuan area of western Henan Province, China. *Acta Geologica Sinica—English Edition* **85**:66–74.

Tanaka, K., D. K. Zelenitsky, H. Saegusa, T. Ikeda, C. L. DeBuhr, and F. Therrien. 2016. Dinosaur eggshell assemblage from Japan reveals unknown diversity of small theropods. *Cretaceous Research* **57**:350–363.

Trimby, P., and G. Grellet-Tinner. 2011. Using electron backscatter diffraction to aid identification of fossilized dinosaur eggshells. *Microscopy and Microanalysis* **17**:574–575.

Tyler, C. 1965. A study of the egg shells of the Sphenisciformes. *Journal of Zoology* **147**:1–19.

Varricchio, D. J., and F. D. Jackson. 2004. A phylogenetic assessment of prismatic dinosaur eggs from the Cretaceous Two Medicine Formation of Montana. *Journal of Vertebrate Paleontology* **24**:931–937.

Vila, B., A. G. Sellés, and J.-C. Beetschen. 2017. The controversial Les Labadous eggshells: a new and peculiar dromaeosaurid (Dinosauria: Theropoda) ootype from the Upper Cretaceous of Europe. *Cretaceous Research* **72**:117–123.

Wang, Q., X.-L. Wang, Z.-K. Zhao, and Y.-G. Jiang. 2010a. A new oogenus of Elongatoolithidae from the Upper Cretaceous Chichengshan Formation of Tiantai Basin, Zhejiang Province. *Vertebrata PalAsiatica* **48**:111–118.

Wang, Q., Z. Zhao, X. Wang, Y. Jiang, and S. Zhang. 2010b. A new oogenus of macroelongatoolithid eggs from the Upper Cretaceous Chichengshan Formation of the Tiantai Basin, Zhejiang Province and a revision of the macroelongatoolithids. *Acta Palaeontologica Sinica* **49**:73–86.

Wang, Q., Z. Zhao, X. Wang, N. Li, and S. Zou. 2013. A new form of Elongatoolithidae, *Undulatoolithus pengi* oogen. et oosp. nov. from Pingxiang, Jiangxi, China. *Zootaxa* **3746**:194–200.

Wang, S., S. Zhang, C. Sullivan, and X. Xu. 2016. Elongatoolithid eggs containing oviraptorid (Theropoda, Oviraptorosauria) embryos from the Upper Cretaceous of Southern China. *BMC Evolutionary Biology* **16**:67.

Weishampel, D. B., D. E. Fastovsky, M. Watabe, D. Varricchio, F. Jackson, K. Tsogtbaatar, and R. Barsbold. 2008. New oviraptorid embryos from Bugin-Tsav, Nemegt Formation (Upper Cretaceous), Mongolia, with insights into their habitat and growth. *Journal of Vertebrate Paleontology* **28**:1110–1119.

Wu, H.-J., Y.-C. Tseng, S.-H. Tsao, P.-L. Chiang, W.-Y. Tai, H.-I. Hsieh, H.-T. Yu, and J.-Y. Juang. 2023. A comparative study on the microstructures, mineral content, and mechanical properties of non-avian reptilian eggshells. *Biology* **12**:688.

Xing, L., K. Niu, W. Ma, D. K. Zelenitsky, T.-R. Yang, and S. L. Brusatte. 2022. An exquisitely preserved in-ovo theropod dinosaur embryo sheds light on avian-like prehatching postures. *iScience* **25**:103516.

Xu, L., J. Xie, S. Zhang, S. Choi, N.-H. Kim, D. Gao, X. Jin, S. Jia, and Y. Gao. 2022. Fossil turtle eggs from the Upper Cretaceous Gaogou Formation, Xiaguan-Gaoqiu Basin, Neixiang County, Henan Province, China: Interpretation of the transformation from aragonite to calcite in fossil turtle eggshell. *Cretaceous Research* **134**:105166.

Yang, T.-R., J. Wiemann, L. Xu, Y.-N. Cheng, X. Wu, and M. Sander. 2019. Reconstruction of oviraptorid clutches illuminates their unique nesting biology. *Acta Palaeontologica Polonica* **64**:581–596.

Young, C.-C. 1954. Fossil reptilian eggs from Laiyang, Shantung, China. *Scientia Sinica* **3**:505–522.

Young, C.-C. 1965. Fossil eggs from Nanhsiung, Kwangtung and Kanchou, Kiangsi. *Vertebrata PalAsiatica* **9**:159–170.

Zelenitsky, D. K., and W. J. Sloboda. 2005. Eggshells. Pp. 398–404 *in* P. J. Currie and E. B. Koppelhus, eds. *Dinosaur provincial park: a spectacular ancient ecosystem revealed*. Indiana University Press, Bloomington.

Zelenitsky, D. K., and F. Therrien. 2008. Unique maniraptoran egg clutch from the Upper Cretaceous Two Medicine Formation of Montana reveals theropod nesting behaviour. *Palaeontology* **51**:1253–1259.

Zelenitsky, D. K., L. V. Hills, and P. J. Currie. 1996. Parataxonomic classification of ornithoid eggshell fragments from the Oldman Formation (Judith River Group; Upper Cretaceous), southern Alberta. *Canadian Journal of Earth Sciences* **33**:1655–1667.

Zelenitsky, D. K., K. Carpenter, and P. J. Currie. 2000. First record of elongatoolithid theropod eggshell from North America: the Asian oogenus *Macroelongatoolithus* from the Lower Cretaceous of Utah. *Journal of Vertebrate Paleontology* **20**:130–138.

Zhao, H., and Z.-K. Zhao. 1999. A new form of elongatoolithid dinosaur eggs from the Lower Cretaceous Shahai Formation of Heishan, Liaoning Province. *Vertebrata PalAsiatica* **37**:278–284.

Zhao, Z. 1975. The microstructure of fossil dinosaur eggs from Nanxiong County, Guangdong Province: concurrent with a discussion on the problem of the classification of dinosaur eggs. *Vertebrata PalAsiatica* **13**:105–117.

Zhao, Z., Q. Wang, and S. Zhang. 2015. Dinosaur eggs. Pp. 1–163 *in Palaeovertbrata Sinica*, Vol. 2. Science Press, Beijing.

Zhu, X., K. Fang, Q. Wang, L. Deng, Y. Liu, J. Wen, X. Wang, and X. Wang. 2021. The first Similifaveoloolithidae (*Wormoolithus luxiensis* oogen. et oosp. nov.) from the Upper Cretaceous of Jiangxi Province, China. *Historical Biology* **33**:689–698.